

SUPPORTING INFORMATION

Structure, optoelectronic properties and thermal stability of the triple organic cations $\text{GA}_x\text{FA}_x\text{MA}_{1-2x}\text{PbI}_3$ system prepared by mechanochemical synthesis

F. B. Minussi¹, L. A. Silva², E. B. Araújo¹

¹ Department of Physics and Chemistry, São Paulo State University, 15385-000 Ilha Solteira, Brazil

² Department of Engineering, University of Rio Verde, 75901-970 Rio Verde, Brazil

Supplementary Note 1: Starting materials and elemental compositions

Table S1 - Quantities of reagents used in the synthesis and the obtained masses of each composition. The yields are relative to the theoretical intended value of 1.4 g of each composition.

Composition	PbI ₂ (g)	MAI (g)	FAI (g)	GAI (g)	Final mass (g)	Yield (%)
$x = 0.00$	1.040	0.361	-	-	1.226	87.6
$x = 0.02$	1.039	0.344	0.008	0.008	1.213	86.6
$x = 0.04$	1.038	0.330	0.015	0.017	1.329	94.9
$x = 0.06$	1.036	0.314	0.023	0.025	1.294	92.4
$x = 0.08$	1.035	0.300	0.031	0.033	1.295	92.5
$x = 0.10$	1.035	0.286	0.038	0.043	1.309	93.5
$x = 0.12$	1.034	0.271	0.046	0.050	1.252	89.4
$x = 0.15$	1.030	0.249	0.058	0.063	1.313	93.8

Table S2 - Carbon, nitrogen, iodine and lead mass content for each GA_xFA_xMA_{1-2x}PbI₃ composition and the calculated iodide to lead molar ratio. Estimations based on EDX analyses of 500x magnified regions.

Composition	C mass %	N mass %	I mass %	Pb mass %	I/Pb molar ratio
$x = 0.00$	3.47 ± 0.52	2.60 ± 0.60	61.20 ± 0.66	32.73 ± 0.53	3.05 ± 0.06
$x = 0.02$	2.61 ± 0.54	2.25 ± 0.61	62.01 ± 0.68	33.13 ± 0.54	3.06 ± 0.06
$x = 0.04$	2.75 ± 0.54	1.94 ± 0.60	62.08 ± 0.68	33.23 ± 0.54	3.05 ± 0.06
$x = 0.06$	2.38 ± 0.57	2.48 ± 0.65	61.74 ± 0.71	33.40 ± 0.56	3.02 ± 0.06
$x = 0.08$	2.73 ± 0.55	2.30 ± 0.62	61.98 ± 0.70	32.98 ± 0.56	3.07 ± 0.06
$x = 0.10$	2.28 ± 0.56	2.08 ± 0.63	61.49 ± 0.69	34.15 ± 0.55	2.94 ± 0.06
$x = 0.12$	2.73 ± 0.56	3.85 ± 0.66	62.08 ± 0.71	31.34 ± 0.56	3.23 ± 0.07
$x = 0.15$	2.45 ± 0.56	1.62 ± 0.64	62.20 ± 0.71	33.73 ± 0.56	3.01 ± 0.06

Supplementary Note 2: Differential scanning calorimetry data and analysis

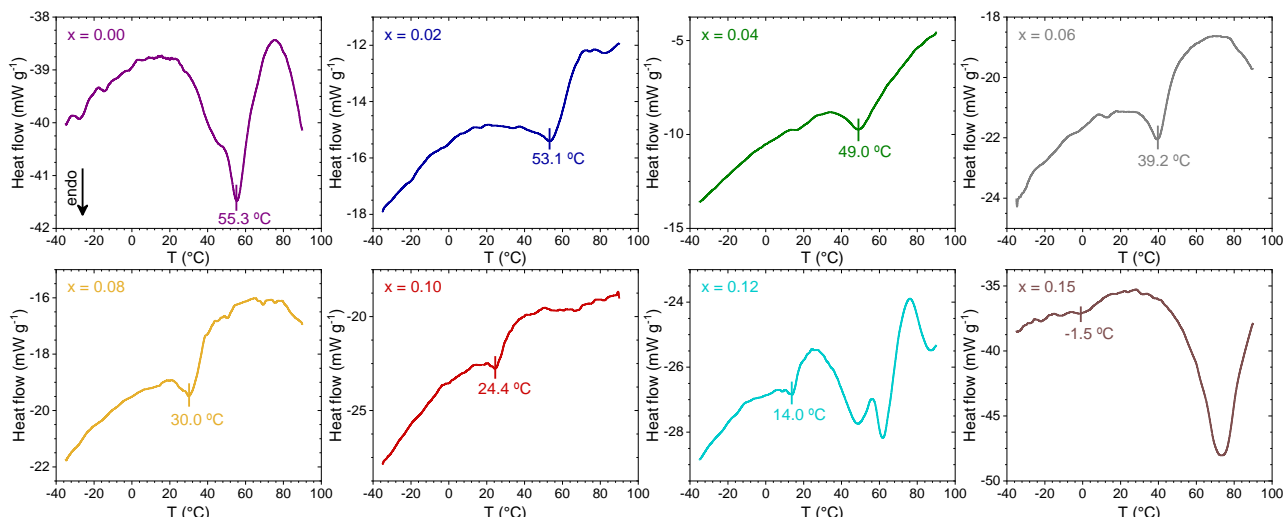


Fig. S1 - Heating DSC curves of the $\text{GA}_x\text{FA}_x\text{MA}_{1-2x}\text{PbI}_3$ powders evidencing possible phase transitions and their respective approximate temperature.

To estimate the transition enthalpies (ΔH_{trans}) on each composition, we calculated the area of the peak attributed to the tetragonal-to-cubic transition on a heat flow vs time DSC curve, shown in Fig. S2. Then, the ΔH_{trans} values (in J mol^{-1}) were obtained using the relation $\Delta H_{trans} = A_p \cdot MM$, where A_p is the peak area and MM is the molar mass of each $\text{GA}_x\text{FA}_x\text{MA}_{1-2x}\text{PbI}_3$ composition. Results are given in the Table S3.

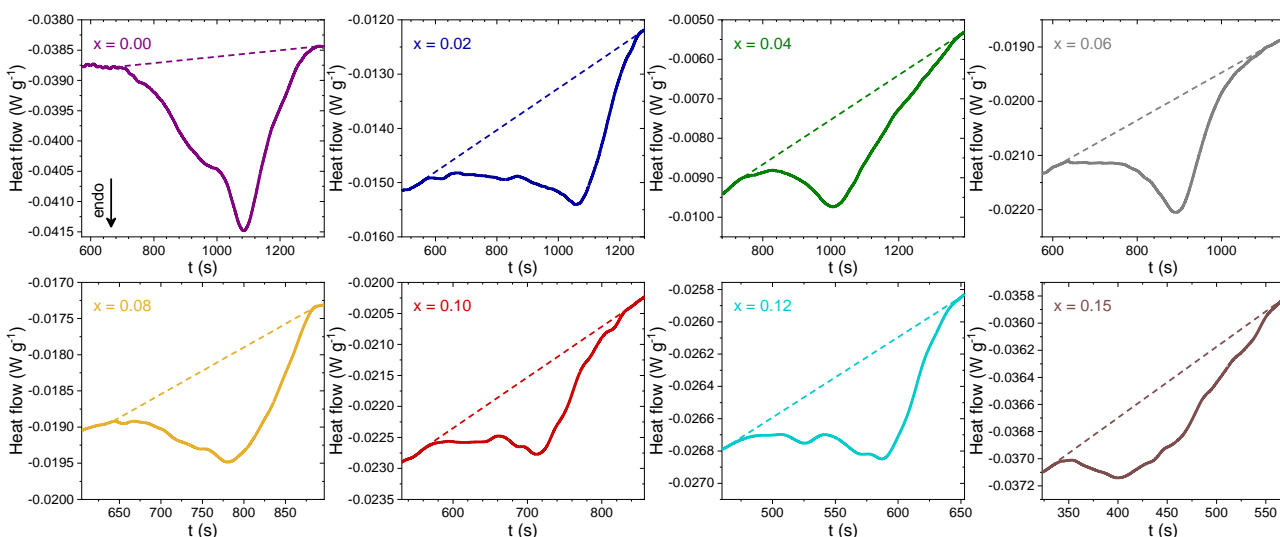


Fig. S2 - Heat flow as a function of time DSC data in the region attributed to the tetragonal-to-cubic phase transition. Dashed lines are the baselines delimiting the peak area calculations.

Table S3 - Results on estimating tetragonal-to-cubic phase transition enthalpies of the $\text{GA}_x\text{FA}_x\text{MA}_{1-2x}\text{PbI}_3$ compositions.

Composition	A_p (J g⁻¹)	MM (g mol⁻¹)	ΔH_{trans} (J mol⁻¹)
$x = 0.00$	0.7293	619.98	452
$x = 0.02$	0.7344	620.80	456
$x = 0.04$	0.5849	621.62	364
$x = 0.06$	0.3552	622.44	221
$x = 0.08$	0.1851	623.26	115
$x = 0.10$	0.1498	624.08	93.5
$x = 0.12$	0.0529	624.90	33.0
$x = 0.15$	0.0636	626.13	39.8

Supplementary Note 3: XRD data fittings of as-synthesized powders

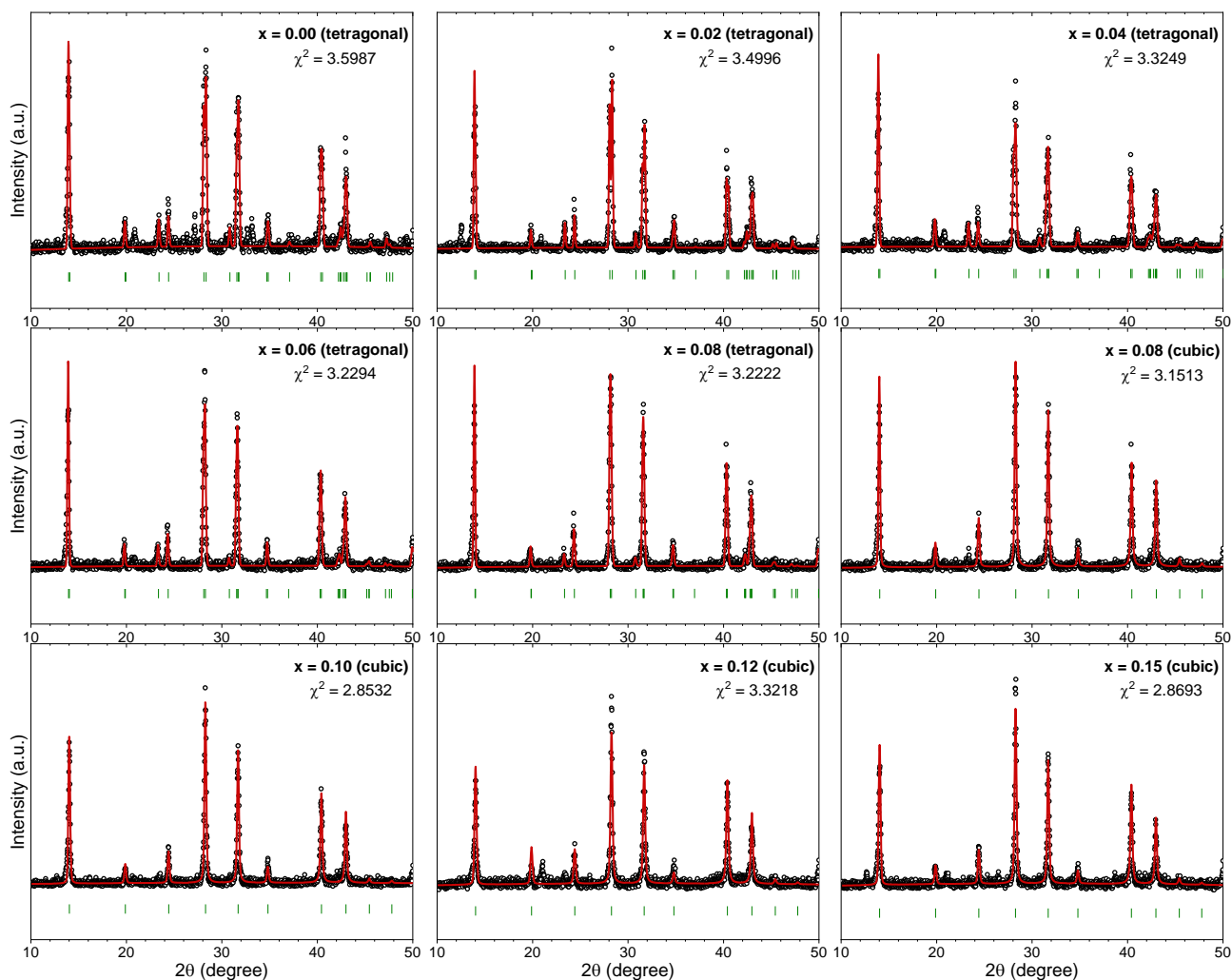


Fig. S3 - Experimental (black circles) and calculated (red lines) XRD data used for the calculation of lattice parameters of the as-synthesized $\text{Ga}_x\text{FA}_x\text{MA}_{1-2x}\text{PbI}_3$ compositions. Green vertical segments are the Bragg positions for $I4cm$ (tetragonal) and $Pm\bar{3}m$ (cubic) space groups. The χ^2 values were given by the FullProf software (march 2021 version).

Table S4 - Results on the lattice parameters obtained through the fits of Fig. S3.

Composition	Tetragonal		Cubic
	a (Å)	c (Å)	a (Å)
$x = 0.00$	8.894(8)	12.683(1)	-
$x = 0.02$	8.894(0)	12.687(7)	-
$x = 0.04$	8.904(7)	12.684(8)	-
$x = 0.06$	8.918(3)	12.682(6)	-
$x = 0.08$	8.924(0)	12.672(7)	6.302(5)
$x = 0.10$	-	-	6.304(7)
$x = 0.12$	-	-	6.308(6)
$x = 0.15$	-	-	6.308(7)

As briefly discussed in the main text, apart from minor PbI_2 signals in $x = 0.02$ and $x = 0.15$ compositions, no signals related to the other precursors or possible by-products are noticed. However, some small peaks can be seen in almost all compositions, where we cite mainly the consistent one at $\sim 21^\circ$. This peak is due to the sample holder used in our measurements. We believe that some other small peaks eventually present might be due to complex hydrides formed during the powder grinding synthesis procedure (which was not conducted under controlled atmosphere) and that were not eliminated during the annealing step. The formation of hydrated perovskites is reported to start within minutes upon some humidity exposure [1].

Supplementary Note 4: Tolerance factors

To obtain a qualitative view on the effects of the substituting cations on the stable perovskite structure, we employed the so-called Goldschmidt tolerance factor (t), given by

$$t = \frac{r_A + r_I}{\sqrt{2}(r_{Pb} + r_I)}$$

where r_i , for $i = A, Pb$ and I , respectively, is the radii of ions in the perovskite $APbI_3$. Since the cations in the A-site are mixed, we used a mean value for each composition, given by

$$r_A = (1 - 2x)r_{MA} + x(r_{GA} + r_{FA})$$

where r_{MA} , r_{GA} , and r_{FA} are the radius of MA^+ , GA^+ and FA^+ cations, respectively, and x is the molar fraction in $GA_xFA_xMA_{1-2x}PbI_3$. For the estimations, we used $r_I = 220$ pm, $r_{MA} = 217$ pm, $r_{GA} = 278$ pm, $r_{FA} = 253$ pm [2], and $r_{Pb} = 119$ pm [3]. The results are given in Fig. S4.

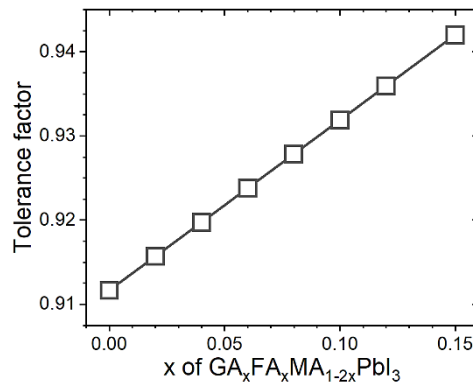


Fig. S4 - Calculated Goldschmidt tolerance factor as a function of the substitution cation content.

Roughly, for values of t in the range from 0.9 to 1.0, mostly cubic perovskites are found. In the 0.80 to 0.89 range, the observed perovskite structures are predominantly characterized by distorted (tilted) octahedral, such as tetragonal and orthorhombic structures [2]. From that perspective, pure $MAPbI_3$ would be on the limit from a tetragonal-to-cubic structure, which is somewhat in accordance with the observed tetragonal structure stable at room temperature. As the value of x is increased, the tolerance factor shifts progressively into the stable cubic structure range. Hence, one could expect a tendency of the cubic structure being preferred over the tetragonal as the substituting cation content is increased, in line with the decreasing tetragonal-to-cubic temperature transition obtained in the present study.

Supplementary Note 5: FTIR spectra and determination of band positions and intensities

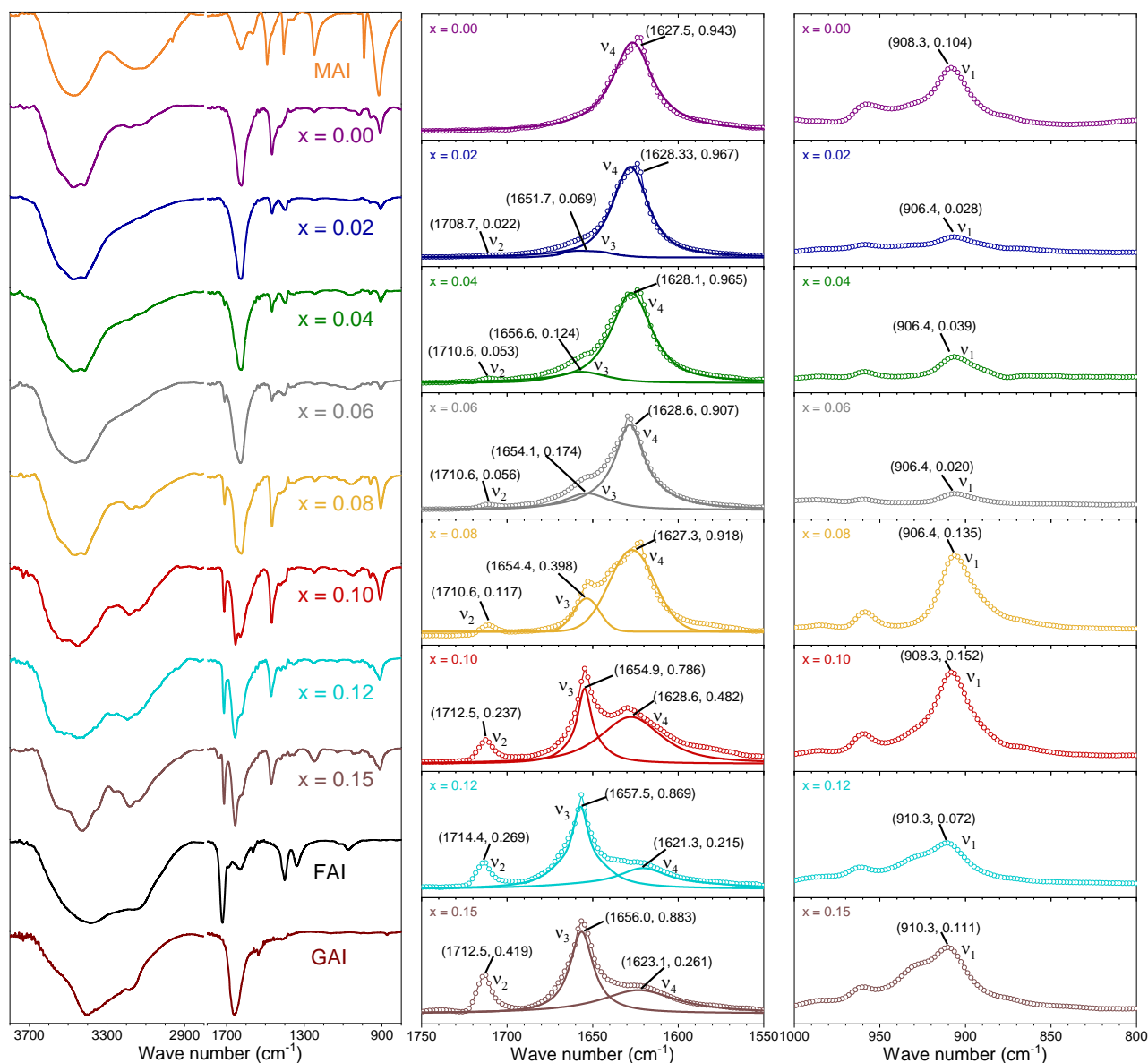


Fig. S5 - Left: normalized transmittance spectra in the regions from 800 to 1800 cm^{-1} and 2800 to 3800 cm^{-1} of each perovskite composition and of organic cation precursors. Right: experimental (circles) and calculated (thick lines) normalized absorbance data used for the determination of intensities and positions of FTIR modes mentioned in the main text. In parentheses, the first number is the position and the second is the relative intensity. For modes ν_1 and ν_2 we used the local maximum points. For modes ν_3 and ν_4 we used the maxima of pseudo-Voigt distributions.

Supplementary Note 6: UV/Vis diffuse reflectance data and analysis

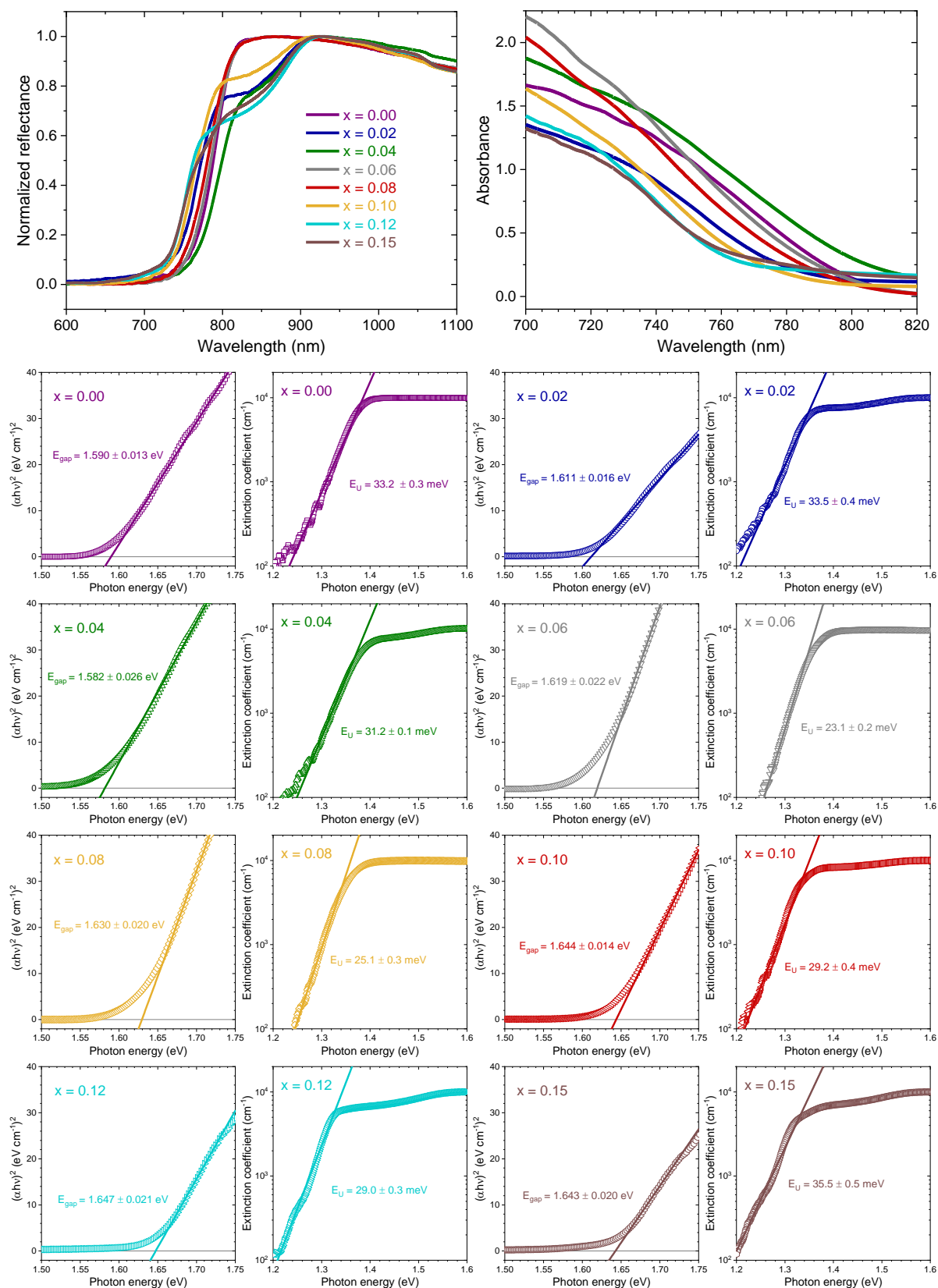


Fig. S6 - Top: normalized reflectance and absorbance spectra in the band gap vicinity. Bottom: Tauc plots and extinction coefficients curves for each composition that were used for the calculation of band gap energies (E_{gap}) and Urbach energies (E_U), respectively. Straight lines are linear fits to the associated equations of each curve.

Supplementary Note 7: XRD data after thermal treatments

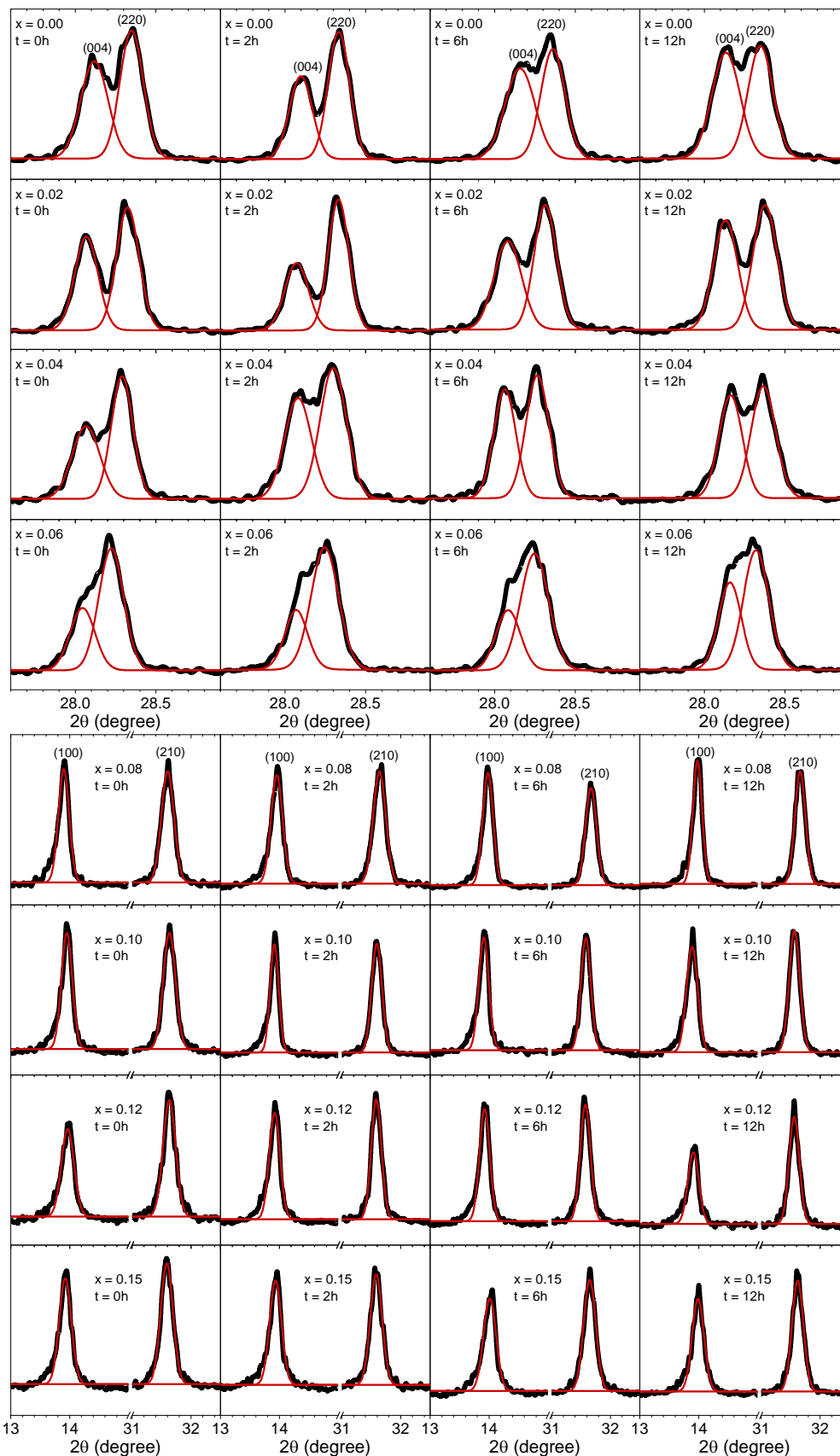


Fig. S7 - Experimental XRD data (black) and calculated Gaussians (red) used for the calculation of peak intensities. Top are of tetragonal and bottom are of cubic structures, respectively.

References

- ¹ P. E. Marchezi et al., *Journal of Materials Chemistry A*, 2020, **8**, 9302.
- ² G. Kieslich et al., *Chemical Science*, 2014, **5**, 4712.
- ³ R. D. Shannon, *Acta Crystallographica Section A*, 1976, **32**, 751.